Qing N.Chan, Paul R.Medwell, Zeyad T.Alwahabi, Bassam B.Dally, Graham

J.Nathan

Assessment of interferences to nonlinear two-line atomic fluorescence (NTLAF) in sooty flames

Applied Physics B: Lasers and Optics, 2011; 104(1):189-198

Applied Physics B: Lasers and Optics manuscript No.
(will be inserted by the editor)

Assessment of Interferences to Nonlinear Two-line Atomic Fluorescence (NTLAF) in Sooty Flames

Qing N. Chan[1,3] ⋆, Paul R. Medwell[2,3], Zeyad T. Alwahabi[1,3], Bassam B. Dally[2,3] and Graham J. Nathan[2,3]

[1] School of Chemical Engineering, The University of Adelaide, S.A. 5005 Australia

[2] School of Mechanical Engineering, The University of Adelaide, S.A. 5005 Australia

[3] Centre for Energy Technology, The University of Adelaide, S.A. 5005 Australia

Received: date / Revised version: date

Abstract Nonlinear excitation regime two-line atomic fluorescence (NTLAF) is a laser-based thermometry technique that has application in turbulent flames with soot. However, no assessment of the various interferences from soot or its precursors in flames with high soot loadings on the technique is available. To examine these issues, both on- and off-wavelength NTLAF measurements are presented and compared for laminar nonpremixed ethylene-air flames. Laser-induced incandescence (LII) measurements were used to determine the corresponding soot concentration and location in the investigated flames. The measurements indicate that interferences, such as spurious scattering and laser-induced incandescence from soot, are not significant for the present set of flame conditions. However, interferences from soot precursors, predominantly condensed species (CS) and perhaps polycyclic aromatic hydrocarbons (PAH), can be significant. Potential detection schemes to correct or circumvent these interference issues are also presented.

Key words Temperature – Soot – Two-line atomic fluorescence – Laser-induced Incandescence – Interferences

1 Introduction

The role of soot in combustion is important due to its environmental and health impacts [1,2], in addition to its role in radiative heat transfer in various combustion systems [3–5]. While combustion processes involving soot have been applied for many years, the formation and

⋆ e-mail: qing.chan@adelaide.edu.au

destruction of soot in practical environments, particularly those that involved turbulent flows, are still beyond the present capacity to model adequately [6]. Comprehensive studies to understand the chemical and physical processes involved in soot formation and destruction in such systems are therefore important. A multitude of interdependent factors are fundamental to the understanding of soot. Of these, temperature, which characterizes the heat transfer process and controls the chemical and physical processes within a flame, is of primary significance.

Laser diagnostics are well-suited to provide *in situ* instantaneous, non-intrusive, temporally and spatially precise measurements of many important parameters of interest [7]. Application of common laser diagnostics in flames containing soot, however, has been problematic due to various interference issues such as absorption and scattering [8]. These issues lead to the application of laser diagnostics often being restricted to idealised clean flames, thus excluding many flames of practical significance. There is therefore a need to develop alternative laser diagnostic methods to complement and to extend those already in common use.

Two-line Atomic Fluorescence (TLAF), with indium as the seeded thermometric species [9,10], is one of the laser diagnostic techniques that have been shown to hold promise in sooting environments. The inelastic nature of the technique enables optical filtering to be used to minimise spurious scattering, thus allowing temperature measurements to be performed in strongly scattering (*e.g.* particle-laden) environments. By extending the technique into the nonlinear excitation regime, the authors have shown that the TLAF signal can be increased sufficiently to enable single-shot imaging [11–14]. Nonlinear excitation regime two-line atomic fluorescence (NTLAF) has also been shown to provide significant improvement on the signal-to-noise ratio (SNR) and hence better precision when compared to the conventional linear regime approach [13].

The NTLAF technique has been shown to provide accurate temperature measurements in lightly sooty flames [13]. However, the capacity of NTLAF to perform temperature measurements in flames with higher soot loadings is yet to be assessed. Such assessments are required because the extent of interference from spurious scattering, laser-induced incandescence and/or fluorescence from soot precursors [15] can be expected to increase with the soot loading within the flame.

To meet these needs, the aim of the present work is to assess the capacity of the NTLAF technique in flames with high soot loadings. Specifically, the present paper aims to compare the measurements, for both Stokes and anti-Stokes processes, when induced at two different laser wavelengths in these flames. The measurements, when induced on-wavelength, are comprised of the indium fluorescence signal and any induced interferences; while the off-wavelength measurements are derived from the extraneous interferences from non-indium source(s). The

present work also aims to determine the role of soot in the interference through the simultaneous application of laser-induced incandescence (LII) to determine the corresponding concentration and location of the soot. It aims to assess these issues for a range of operating laser fluences and flame stoichiometries in the present paper.

2 Methodology

The TLAF process involves the sequentially shifted measurements of Stokes and anti-Stokes direct-line fluorescence produced from the optical excitation of a three-level system, namely the indium atom [9]. The three energy levels of a neutral indium atom that are relevant to TLAF are shown in Fig. 1.

The Stokes process involves 410.18 nm laser excitation ($5^2P_{1/2} \rightarrow 6^2S_{1/2}$ transition), and the subsequent fluorescence ($6^2S_{1/2} \rightarrow 5^2P_{3/2}$ transition) is detected at 451.13 nm. The anti-Stokes process uses 451.13 nm excitation ($5^2P_{3/2} \rightarrow 6^2S_{1/2}$ transition) and 410.18 nm detection ($6^2S_{1/2} \rightarrow 5^2P_{1/2}$ transition). The flame temperature is subsequently deduced from the ratio of these fluorescence signals. A full description of the TLAF theory, especially incorporating NTLAF, has been presented in a previous publication [13].

3 Experimental

3.1 Burner details

Laminar nonpremixed flames were chosen for the present study since soot is formed readily in such combustion environments, whilst avoiding complications associated with the presence of turbulence [12, 16]. Additionally, nonpremixed flames typically have distinct regions that assist in identification of any source(s) of extraneous interferences based on spatial position in reaction zone. A Jet in Hot Co-flow (JHC) style burner [17] was used in the present study to generate the laminar nonpremixed flames required.

The burner consists of a central fuel jet (⌀=20 mm) within an annular co-flow (⌀=110 mm). The fuel jet exit consists of a perforated stainless steel disc with equally-spaced holes (⌀=0.8 mm). The design of this plate facilitates the seeding of an aerosol containing indium chloride. A co-flow gas of either nitrogen, air or a premixture of fuel and air can be employed, but only an air co-flow was used for the present study. The flow-conditioning of the co-flow gas stream was achieved with the use of stainless steel mesh and layers of flint clay.

Industrial grade ethylene (>99.5 % C_2H_4) was used as the fuel for the present investigation. A portion of the fuel was passed through a seeder to facilitate the seeding of indium into the fuel stream. The seeder, which consists of an ultrasonic nebuliser within a chamber, was used to generate a mist of droplets of indium chloride dissolved

in methanol. The concentration of the indium chloride salt in the solution was chosen to be 1.125 mg/mL. This concentration was selected to provide an optimal signal while avoiding absorption and signal trapping. A ballast volume was included between the seeder and the burner to damp variations in the aerosol generation [18].

The parameters of the fuel stream at the exit of the central fuel jet, issuing into a fixed air co-flow with a bulk velocity of 1.5×10^{-3} m/s, are shown in Table 1. In the present study, the stoichiometry (Φ) of the flames was varied by adjusting the air flow rate with a constant fuel flow rate. This maintains a similar amount of seeded indium within each of the flames. The low flow rates employed resulted in flames of spatially wide reaction zones with discernible features, which is advantageous for the purposes of the present study.

3.2 Laser systems details

The experimental arrangement used for the present investigation follows that described previously [12]. A schematic diagram of the experimental layout is shown in Fig. 2.

3.2.1 NTLAF experimental details In brief, two Nd:YAG pumped dye lasers were tuned to 410.18 nm and 451.13 nm respectively, for on-wavelength measurements, and 412 nm and 454 nm respectively, for off-wavelength measurements. The laser pulses were fired with ∼100 ns separation. The two beams were circularly polarised and combined into co-planar laser sheets of ∼0.3 mm thickness through the measurement volume. The laser sheets were directed through a tank, which was filled with fluorescing dye, in the same field of view as the burner. This is to allow for shot-by-shot correction of the laser energy and profile variation across sheet height. The frequency-shifted emissions from both the tank and the flame were detected through 450 nm and 410 nm optical filters (both with 10 nm bandwidth), using $f_{\#}1.4$ lenses, onto two intensified CCD (ICCD) cameras. The gate widths of the cameras were set to 50 ns. The timings of the cameras were set to be prompt with laser excitation.

3.2.2 LII experimental details An Nd:YAG laser operating at 1064 nm was used for the LII excitation. The 1064 nm laser beam shared the same optical pathway as the NTLAF process. The lenses used are not achromatic, leading to a slight difference in the focal length, though insignificant over the region of interest through the flame. The LII laser sheet was 20 mm in height with ∼0.3 mm thickness. The operating laser fluence was maintained at ∼0.5 J/cm^2, which is within the plateau region (not shown), to ensure that LII signals observed are approximately independent of the laser fluence variation [19, 20].

The wings of the sheet exhibiting lower laser fluence were clipped with a rectangular aperture. The LII signal was detected through a 410 nm optical filter (10 nm bandwidth), using a $f_{\#}1.4$ lens, onto another ICCD camera. The gate width of the camera was set to 100 ns

and the timing was set to be prompt to the LII excitation process. This timing scheme was selected to reduce the size-dependent sensitivity of the signal [21]. The LII signals were calibrated using laser extinction measurements. A chopped, continuous-wave 1064 nm beam was used to avoid absorption processes from polycyclic aromatic hydrocarbons (PAH) or similar [22]. The soot extinction coefficient (Ke) was taken to be 9.2, following the work of Williams *et al.* [23].

A delay generator was used to control the relative timing of the lasers and the camera detection gates. The detection and timing schemes employed in the present study have been previously shown to avoid cross-talk between the NTLAF and the LII processes [12]. The LII process was delayed ∼800 ns after the NTLAF measurements. The LII process was set to occur after the NLTAF process since the temporal decay (hundreds of nanoseconds) of the LII signal is slower than that of the fluorescence (tens of nanoseconds) [24]. Also, the ablation of the soot may invoke other influences on the flame.

4 Data processing

The images from all three cameras were spatially matched to sub-pixel accuracy using a four-point matching algorithm and then morphed based on the cross-correlation of a transparent grid image. The in-plane resolution of the images is ∼260 μm. All images presented here have been corrected for background and detector attenuation.

The images presented for this laminar flame system were median-averaged over 150 shots to improve on the SNR. Being a steady laminar flame system, there is no loss of information resulting from the averaging. No pixel binning was performed on the images to prevent degradation of the spatial resolution. It should be noted that, whilst the images presented here have been shot-averaged to achieve the best possible signal quality, the SNR of NTLAF technique has been previously shown to be sufficient to be applied on a single-shot basis [12, 14].

5 Results and Discussion

5.1 On- and off-wavelength measurements

5.1.1 Typical On- and off-wavelength measurements Figure 3 shows the typical averaged on-wavelength measurements (I_{on}) for the (a) Stokes and (b) anti-Stokes processes in Flame 2 (Table 1). These measurements comprise of the signal from the indium fluorescence, and laser-induced interferences from the flame. Both measurements were recorded simultaneously under an operating fluence of ∼0.01 J/cm^2. Figure 3(c) presents the averaged soot volume fraction distribution of the same flame, measured simultaneously with the on-wavelength measurements. The figure shows that the soot volume fraction for Flame 2 peaks at 4.08 ppm. The images presented represent an area of 10 mm high and 30 mm wide, taken at a height above burner (HAB) centred at 25 mm.

Figure 4 shows the typical averaged off-wavelength measurements (I_{off}) for the (a) Stokes and (b) anti-Stokes processes in Flame 2 (Table 1). These images were recorded under the same operating fluence as the on-wavelength measurements; only, the wavelength has been shifted slightly to detune it from the resonance of indium. These images therefore correspond to the extraneous interferences, which would also contribute to the measurements shown in Fig. 3. It is worth noting that even though the on- and off-wavelength measurements were performed at the same laminar flame condition *i.e.* Flame 2, it was not possible to collect these measurements concurrently with the present experimental setup. Their simultaneous measurements would require two additional tunable lasers and cameras.

It is worth noting that the on- and off-wavelength measurements presented here are given in arbitrary units (a.u.) since the strength of the measurements is dependent on the details of the optical arrangement. Nevertheless, a relative comparison of the off-wavelength with the on-wavelength measurements can be made, if the excitation characteristics of the off-wavelength measurements assumed to be sufficiently broadband as to be insensitive to the slight changes in the line width associated with the change in the excitation frequency.

Figure 5 presents an overlay of the on- and off-wavelength measurements from Fig. 3 and Fig. 4 respectively. It is evident that the off-wavelength measurements overlap a narrow portion on the inner fuel-rich side of the broader on-wavelength measurements. The flame front can be identified from the region of highest intensity in the on-wavelength measurements, since this approximately marks the region with the highest temperature [14]. These observations suggest that the source(s) of the observed off-wavelength measurements is only associated with the fuel-rich side of the reaction zone, and not with the flame front or oxidising region.

Figure 6 shows the overlapping of the off-wavelength measurements and the LII image of soot volume fraction for both the Stokes and anti-Stokes processes. It is apparent that the locations of the off-wavelength measurements are distinct from the the soot regions and are also on the fuel-rich side of the soot sheet. The difference in the locations of the measurements implies that soot interferences, such as spurious scattering and laser-induced incandescence, do not contribute significantly to the off-wavelength measurements. Rather, such spurious scattering from the soot is effectively suppressed by the optical arrangement employed. The observation also indicates that the chosen fluence for these NTLAF measurements avoids soot incandescence, despite operating in the nonlinear excitation regime [13].

It can also be seen from Fig. 6 that the off-wavelength measurements are observed to occur at a similar location for both the Stokes and anti-Stokes processes, suggesting that the same source(s) is likely to be responsible for each. Furthermore, since the off-wavelength measurements are detected for both the Stokes and anti-Stokes

processes, it can be inferred that these laser-induced emissions are characterised by a broad spectral range.

The averaged distribution of the on- and off-wavelength measurements, and of the soot volume fraction are normalised in Fig. 7. These averaged radial profiles were extracted at a HAB of 25 mm, and are normalised to their peak values. From Fig. 7, it can be seen that the off-wavelength measurements peak at a radial location (r) of ∼6.5 mm and has a FWHM spread of ∼2.3 mm. By contrast, the soot particles peak at r≈7.5 mm and are confined to a thinner region (FWHM≈1.3 mm). A close inspection of Fig. 7 also reveals that the off-wavelength measurements peak at the same radial location (r≈6.5 mm) as the onset of the soot. This observation suggests that the source(s) that resulted in the observed off-wavelength measurements participates in the soot formation process, since the consumption of the species coincides with the appearance of the soot particles. It is also consistent with the knowledge that soot precursors are found on the fuel-rich side of the soot layer.

Measurements from both Stokes and anti-Stokes processes are observed to have qualitatively similar characteristics throughout the present study. Hence, only results obtained for the anti-Stokes process are presented and discussed in the subsequent sections.

5.1.2 Effect of laser fluence Figure 8 presents the averaged radial profiles for the on- and off-wavelength measurements in Flame 2 (Table 1) at a HAB of 25 mm, at four different laser fluences. To generate this plot, the laser fluence was varied by the addition of neutral density filters of differing optical density (OD) into the beam. This approach allows the variation in intensity while maintaining consistent optical properties of the beam. Both the flame condition and indium seeding concentration were held constant. The radial location of the peak soot volume fraction is indicated on the figure with a vertical dotted line.

A consistent trend is evident in Fig. 8, with the intensities of both the on- and off-wavelength measurements found to reduce with decreasing laser fluence. In general, each of the on-wavelength measurements is observed to exhibit a qualitatively similar trend. The on-wavelength measurements are observed to peak (air-side peak) at a radial location between the air side and the position of the maximum soot volume fraction. Also, a secondary peak (fuel-side peak) appears at an intermediate position between the soot zone and the fuel-rich side. The off-wavelength measurements exhibit qualitatively similar trends to the findings discussed earlier from Fig. 7.

The peaks for the on-wavelength measurements are observed to display dissimilar trends when different laser fluences are used. For the case of laser fluence = 0.010 J/cm^2 and 0.008 J/cm^2 , the fuel-side peaks are observed to have a higher intensity than the air-side peaks. However, such characteristic does not persist and is found to have inversed for the case at lower laser fluences (*i.e.* laser fluence = 0.003 J/cm^2 and 0.001 J/cm^2). The dif-

ference in the dependency of the air-side and the fuel-side peaks on the laser fluences implies that the observed on-wavelength measurements are comprised of laser-induced emissions from species with dissimilar spectroscopic properties. A close inspection of the radial profiles in Fig. 8 further reveals that the fuel-side peaks of the on- wavelength measurements are in good agreement with profiles of the off-wavelength measurements, with the local maxima of the fuel-side peaks and the off-wavelength measurements occurring at similar radial locations. The likeness of the profiles over the region suggests that the the fuel-side peak of the on-wavelength measurements are mainly comprised of the laser-induced emissions from the same non-indium source(s) responsible for the off-wavelength measurements.

Figure 9 compares the relative magnitude of the maximum off-wavelength to on-wavelength measurements, obtained from Fig. 8, as a function of laser fluence. It is evident from the figure the interference remains significant at all fluences. This observation implies that the laser-induced emissions from the non-indium source(s) are not an artefact of the operating laser fluence of NTLAF and are readily stimulated even at very low fluences.

Polycyclic aromatic hydrocarbons (PAH) [15,24,16, 25] and condensed species (CS) [26–28] have been reported to form readily in fuel-rich zones and are deduced to play important roles in soot formation processes. The emissions from both PAH and CS are characterised by broad spectra range and are reported to exhibit both Stokes (red-shifted) and anti-Stokes (blue-shifted) components [29,30]. The similarities between the characteristics of the off-wavelength measurements and the findings of the previous studies suggest that the laser-induced emissions from PAH and CS should be considered in seeking to identify the cause of the interference. Other studies, however, have reported that PAH emission in the visible spectrum is negligible [27], indicating that CS is more likely to be the species causing the off-wavelength measurements. Nevertheless, it is possible that the spectroscopic properties of the PAH might be influenced by the high temperature flame environment, shifting in the emission significantly towards visible [28,31]. Therefore, the contribution of the PAH emission in perturbing the NTLAF measurements cannot be ruled out completely.

5.1.3 Effect of stoichiometry Figure 10 presents the averaged radial profiles of on- and off-wavelength measurements in Flame 1 to Flame 5 (Table 1) at a fixed operating laser fluence of $\sim$0.01 J/cm^2. Again, these profiles were extracted at a HAB of 25 mm in all flames. Measurements are presented as a function of radial distance from the peak of the soot volume fraction (r'). This identifies the variations relative to the flame front. From Fig. 10, it can be seen that the influence of the fuel-rich interference peak in the on-wavelength measurements is greater in the richer flames than in the

leaner flames. That is, the richer the flame, the more intense the off-wavelength measurements. This is consistent with the deduced importance of PAH and CS since both are formed preferentially under richer conditions.

From Fig. 10, it can be seen that there is an enhancement in the intensity of the on-wavelength measurements, as the flame becomes leaner. This observation appears to be opposite to the general view that the neutral indium atoms are generated more efficiently in fuel-rich zones [32,33]. The processes by which the neutral indium atoms are converted from indium chloride solutions are complex, as described in detail in previous publications [11,14]. In brief, desolvation occurs upon heating near the flame front, leaving the indium in the form of various metal complexes. These complexes subsequently undergo a series of gas-phase reactions to form a variety of species with competing equilibria, one of which is the desired neutral indium atom. Such reactions are highly localised in the flame and are dependent on numerous factors such as the temperature and the chemical compositions of the region [34].

Flame 2 to Flame 5 are fuel-rich flames slightly premixed with air, so have wide reaction zones. The various processes involved in the generation of indium atoms are therefore allowed more time to proceed. Additionally, the efficiency of the desolvation step is also expected to increase in the leaner flames, which have more favorable heat release profiles. The interactions of these two effects may have compensated for the decrease in the efficiency of indium formation in leaner flames. Factors such as the requirement for the activation of indium within flame front [35] or the possible formation of carbon-containing indium compounds in sooty flames, which result in decreased indium atom formation efficiency [34], may also contribute to the observed trends.

It is worth mentioning that, despite an overall enhancement in the intensity of the on-wavelength measurements from fuel-rich to fuel-lean, there is no substantial difference in the general shapes of the profiles. Neglecting the cases such as $\Phi = \infty$ and 31.3, where the on-wavelength measurements are highly perturbed by the extraneous emissions from non-indium sources, all of the curves are found to pass through a maximum at an intermediate position between the soot zone and air side. Again, the shapes of these curves are expected to reflect the composite effects of the various factors discussed previously.

5.2 Potential schemes to correct for or circumvent interferences

5.2.1 Off-wavelength measurements To investigate approaches to correct for the aforementioned interferences, Fig. 11 presents the averaged radial profiles that result from the subtraction of the extraneous interferences, *i.e.* off-wavelength measurements, from the on-wavelength measurements in Fig. 8. It can be seen that each of the averaged radial profiles exhibit qualitative similar trends to the on-wavelength measurements in Fig. 10

that are observed to be least affected by the extraneous interferences (*i.e.* Φ = 4.2 and 5.9). This observation suggests that the off-wavelength measurements can potentially be used to account/correct for the interferences present, over a range of laser fluences. Also, this observation supports the earlier assumption in § 5.1.1 that the off-wavelength measurements are likely to be insensitive to the changes in line width associated with slight detuning of the laser.

5.2.2 Off-resonance measurements To investigate approaches to circumvent the aforementioned interferences, the averaged distribution of the off-resonance and the corresponding off-wavelength measurements in Flame 1 (Table 1) are presented in Fig. 12 for the anti-Stokes process. The LII soot volume fraction distribution for the flame is overlaid as well. The off-resonance measurements were collected with the use of a 430 nm filter (10 nm bandwidth) in conjunction with on-wavelength excitation *i.e.* 450 nm excitation for anti-Stokes process. From Fig. 12, it is evident that the both the off-resonance and off-wavelength measurements show qualitative similar features. It is worth noting that the off-resonance and off-wavelength measurements are found to differ quantitatively, as expected, since different detection optics were used for the collection of each of the measurements. These findings suggest that the off-resonance measurements would be more useful for identification, rather than correction, of the regions of NTLAF images that are identified to be significantly affected by the extraneous interferences present. It is also important to note that the off-resonance and off-wavelength measurements for the Stokes process (not shown here) are found display similar characteristic as well.

5.2.3 Fuel-air ratio Figure 13 presents the dependence on the flame stoichiometry of the maximum off-wavelength to on-wavelength measurements ratios. These data were extracted from the fuel-rich peak between the fuel and soot zones where the off-wavelength measurements are found to be significant. Also presented are the corresponding maximum soot volume fraction (SVF_{max}). It can be seen that there is a strong, although not absolute, correlation between the amount of soot and interference, as expected. Clearly, the relationship between these two parameters is not absolute and will depend on factors such as fuel type and strain [36]. Nevertheless, it is demonstrated that measurements without the need for correction will be possible for flames with sufficiently low yet still useful soot loadings. Specifically, it can be seen that the maximum interference to the total emission ratio is lower than 0.05 when the flame stoichiometry is less than Φ = 9.6 and when the SVF_{max} is $\sim$1.3 ppm for this fuel. Given the expected dependence of this relationship on fuel type and experimental conditions, it is desirable to perform a similar check for specific conditions of interest.

6 Conclusion

This paper has investigated on the contribution of the extraneous interferences from non-indium sources towards the nonlinear two-line atomic fluorescence (NTLAF) measurements in flames with high soot loadings. In conclusion,

- The off-wavelength measurements show that the interference is significant from soot precursors, but not from soot itself.
- Comparison of the spatial locations of the various peaks of the measurements suggest that the interference is derived predominantly from condensed species (CS) and perhaps also from polycyclic aromatic hydrocarbons (PAH).
- The correction of the extraneous interferences with the use of off-wavelength measurements is potentially feasible.
- The identification and elimination of the regions of the NTLAF data that are found to be significantly affected by extraneous interferences with the use of off-resonance measurements is plausible.
- The NTLAF can be expected to perform reliably, without the need for correction, in selected flame conditions with low yet useful soot loadings.

These results also justify more work to directly evaluate the efficacy of the correction schemes on the accuracy of the measurements in flames with high soot loadings. Even an imperfect correction would allow the extension of the usable range of the NTLAF technique to flames of higher soot loadings.

Acknowledgments

The authors wish to acknowledge the support of the Centre for Energy Technology (CET) and The University of Adelaide. The Australian Research Council (ARC) is also gratefully acknowledged for their funding support of this work through ARC Discovery and Linkage Infrastructure, Equipment and Facilities (LIEF) grant schemes. The authors are also grateful to Dr Peter Kalt from the School of Mechanical Engineering and Mr Jason Peak and Mr Jeffrey Hiorns from the Chemical Engineering workshop for their helpful discussions and invaluable assistance during this project.

References

1. D. W. Dockery, P. H. Stone: N. Engl. J. Med. 356(5), 511–513 (2007).
2. N. Künzli, R. Kaiser, S. Medina, M. Studnicka, O. Chanel, P. Filliger, M. Herry, F. H. Jr, V. Puybonnieux-Texier, P. Quénel, J. Schneider, R. Seethaler, J. C. Vergnaud, H. Sommer: The Lancet 356, 795–801 (2000).
3. M. A. Delichatsios, J. D. Ris, L. Orloff: Proc. Combust. Inst. 24, 1075–1082 (1992).
4. G. Nathan, J. Mi, Z. Alwahabi, G. Newbold, D. Nobes: Prog. Energy Combust. Sci. 32, 496–538 (2006).
5. J. J. Parham, G. J. Nathan, J. P. Smart, S. J. Hill, B. G. Jenkins: J. I. Energy 73, 25–34 (2000).

6. Z. A. Mansurov: Combust. Explo. Shock+ 41(6), 727–744 (2005).
7. M. Aldén: Combust. Sci. Technol. 149, 1–18 (1999).
8. A. T. Hartlieb, B. Atakan, K. Kohse-Höinghaus: Appl. Phys. B 70, 435–445 (2000).
9. J. E. Dec, J. O. Keller: Proc. Combust. Inst. 21, 1737–1745 (1986).
10. C. F. Kaminski, J. Engström, M. Aldén: Proc. Combust. Inst. 27, 85–93 (1998).
11. Q. N. Chan, P. R. Medwell, P. A. M. Kalt, Z. T. Alwahabi, B. B. Dally, G. J. Nathan: Appl. Opt. 49(8), 1257–1266 (2010).
12. Q. N. Chan, P. R. Medwell, P. A. Kalt, Z. T. Alwahabi, B. B. Dally, G. J. Nathan: Proc. Combust. Inst. DOI 10.1016/j.proci.2010.06.031 (2010).
13. P. R. Medwell, Q. N. Chan, P. A. M. Kalt, Z. T. Alwahabi, B. B. Dally, G. J. Nathan: Appl. Opt. 48(7), 1237–1248 (2009).
14. P. R. Medwell, Q. N. Chan, P. A. M. Kalt, Z. T. Alwahabi, B. B. Dally, G. J. Nathan: Appl. Spectrosc. 64(2), 173–176 (2010).
15. C. S. Moreau, E. Therssen, X. Mercier, J. F. Pauwels, P. Desgroux: Appl. Phys. B 78, 485492 (2004).
16. A. Gomez, M. G. Littman, I. Glassman: Combust. Flame 70, 225–241 (1987).
17. P. R. Medwell, P. A. M. Kalt, B. B. Dally: Combust. Flame 152, 100–113 (2008).
18. R. K. Winge, V. A. Fassel, R. N. Kniseley: Appl. Spectrosc. 25(6), 636–642 (1971).
19. C. Schultz, B. F. Kock, M. Hofmann, H. Michelsen, S. Will, B. Bougie, R. Suntz, G. Smallwood: Appl. Phys. B 83, 333–354 (2006).
20. N. H. Qamar, Z. T. Alwahabi, Q. N. Chan, G. J. Nathan, D. Roekaerts, K. D. King: Combust. Flame 156, 1339–1347 (2009).
21. R. L. V. Wal: Appl. Opt. 35(33), 6548–6559 (1996).
22. J. Zerbs, K. P. Geigle, O. Lammel, J. Hader, R. Stirn, R. Hadef, W. Meier: Appl. Phys. B 96, 683–694 (2009).
23. T. C. Williams, C. R. Shaddix, K. A. Jensen, J. M. Auo-Antilla: Int. J. Heat Mass Transfer 50, 1616–1630 (2007).
24. R. L. V. Wal, K. A. Jensen, M. Y. Choi: Combust. Flame 109, 399–414 (1997).
25. G. Prado, A. Garo, A. Ko, A. Sarofim: Proc. Combust. Inst. 20, 989–996 (1984).
26. A. Ciajolo, A. D'Anna, R. Barbella: Combust. Sci. Technol. 100(1), 271–281 (1994).
27. A. Ciajolo, R. Ragucci, B. Apicella, R. Barbella, M. de Joannon, A. Tregrossi: Chemosphere 42, 835–841 (2001).
28. A. Ciajolo, B. Apicella, R. Barbella, A. Tregrossi, F. Beretta, C. Allouis: Energy Fuels 15, 987–995 (2001).
29. F. Beretta, V. Cincotti, A. D'Alessio, P. Menna: Combust. Flame 61, 211–218 (1985).
30. L. Petarca, F. Marconi: Combust. Flame 78, 308–325 (1989).
31. D. S. Coe, J. I. Steinfeld: Chem. Phys. Lett. 76(3), 485–489 (1980).
32. J. Engström, J. Nygren, M. Aldén, C. F. Kaminski: Opt. Lett. 25(19), 1469–1471 (2000).
33. J. Nygren, J. Engström, J. Walewski, C. F. Kaminski, M. Aldén: Meas. Sci. Technol. 12, 1294–1303 (2001).
34. V. A. Fassel, J. O. Rasmuson, R. N. Kniseley, T. G. Cowley: Spectrochim. Acta 25B, 559–575 (1970).

35. W. G. Bessler, F. Hildenbrand, C. Schulz: Appl. Opt. 40(6), 748–756 (2001).

36. B. S. Haynes, H. G. Wagner: Prog. Energy Combust. Sci. 7, 229–273 (1981).

Table 1 Parameters of the fuel stream at the exit of the central fuel jet, issuing into a fixed air co-flow, for the flame conditions of interest.

Flame Number	Fuel stream	Stoichiometry (Φ)	Bulk velocity (m/s)	Percentage O_2 (% vol.)
1	Ethylene	∞	0.63	0.0
2	Ethylene & air	31.3	0.91	6.3
3	Ethylene & air	9.6	1.53	12.3
4	Ethylene & air	5.9	2.09	14.6
5	Ethylene & air	4.2	2.68	16.0

List of Figures

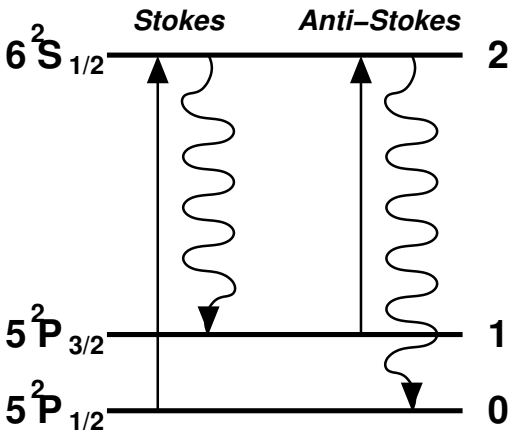

Fig. 1 Indium atom energy transitions involved in Two-Line Atomic Fluorescence (TLAF).

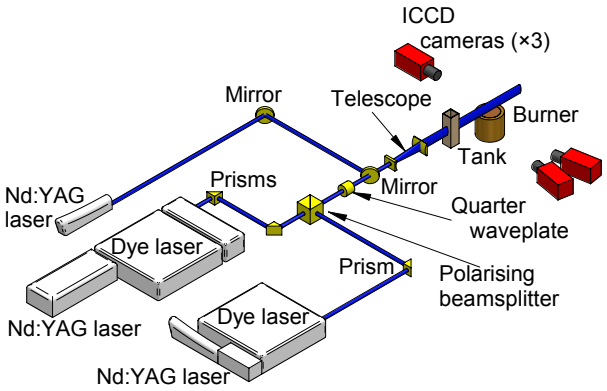

Fig. 2 Schematic diagram of the experimental arrangement.

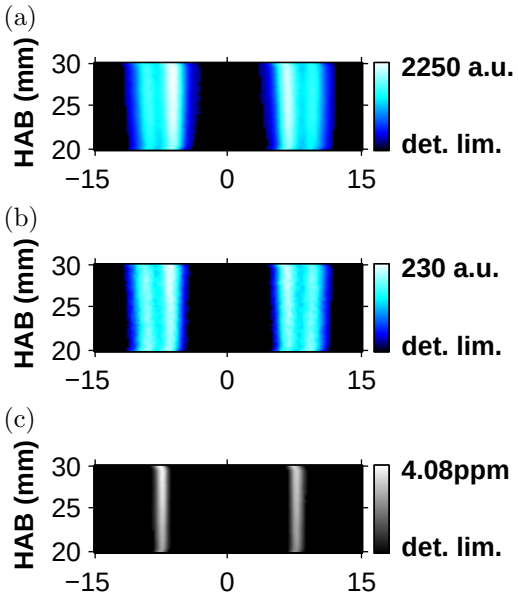

Fig. 3 (Color online) Typical averaged on-wavelength (a) Stokes, (b) anti-Stokes measurements and (c) LII soot volume fraction distribution in Flame 2 (Table 1).

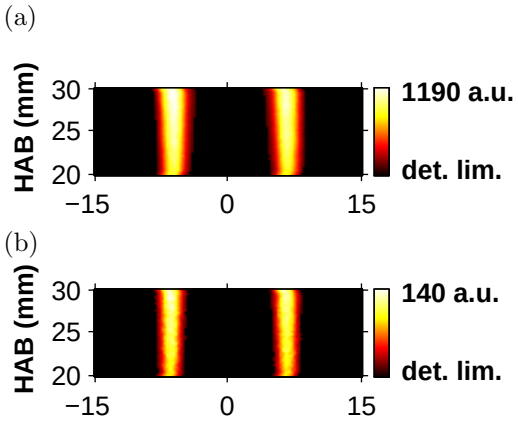

Fig. 4 (Color online) Typical averaged off-wavelength (a) Stokes and (b) anti-Stokes measurements in Flame 2 (Table 1).

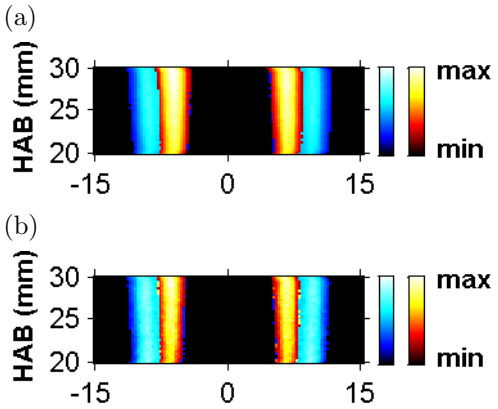

Fig. 5 (Color online) Typical averaged on-wavelength measurements, with off-wavelength measurements overlaid for (a) Stokes and (b) anti-Stokes processes in Flame 2 (Table 1). On-wavelength: Blue—White. Off-wavelength: Red—White.

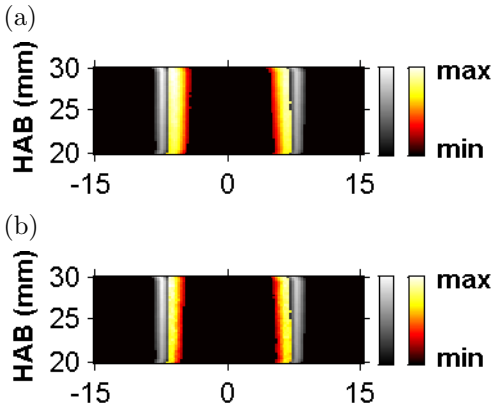

Fig. 6 (Color online) Typical averaged off-wavelength measurements with LII soot volume fraction overlaid for (a) Stokes and (b) anti-Stokes processes in Flame 2 (Table 1). Soot: Grey—White. Off-wavelength: Red—White.

(a)

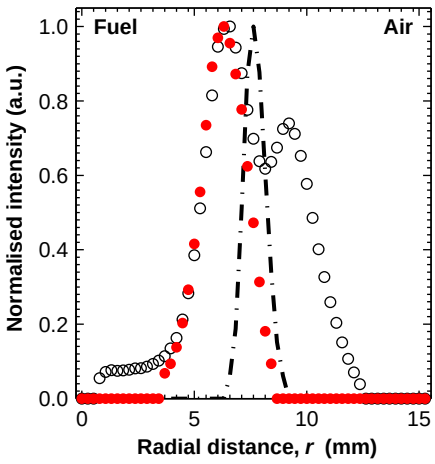

(b)

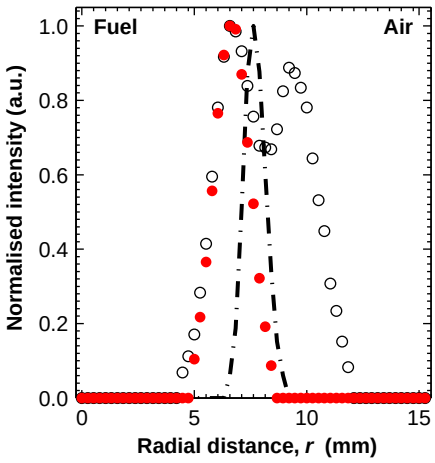

Fig. 7 Average radial profiles for the (a) Stokes and (b) anti-Stokes processes extracted at a HAB of 25 mm in Flame 2 (Table 1). Open circles: on-wavelength measurements. Dots: off-wavelength measurements. Dashed line: soot volume fraction. These radial profiles have been normalised arbitrarily to their peak values.

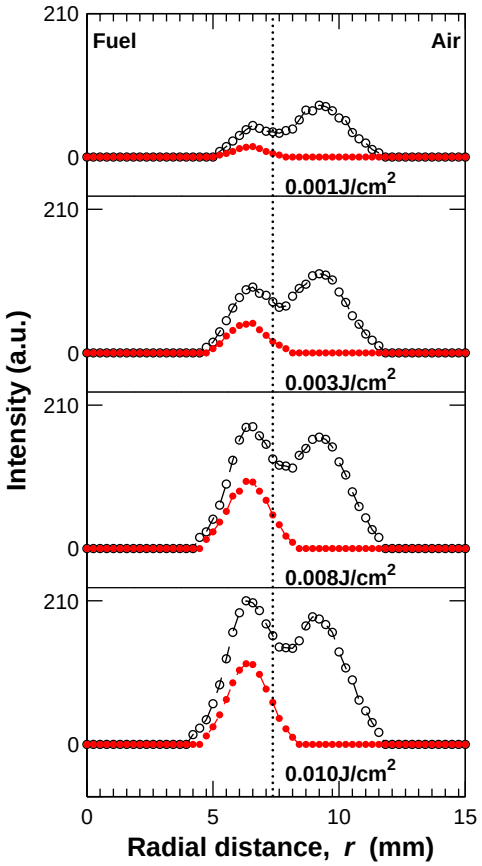

Fig. 8 Averaged radial profiles for the on-wavelength measurements at four different laser fluences, extracted at a HAB of 25 mm in Flame 2 (Table 1). Anti-Stokes process. Open circles: on-wavelength measurements. Dots: off-wavelength measurements. Vertical dotted line: peak soot volume fraction location.

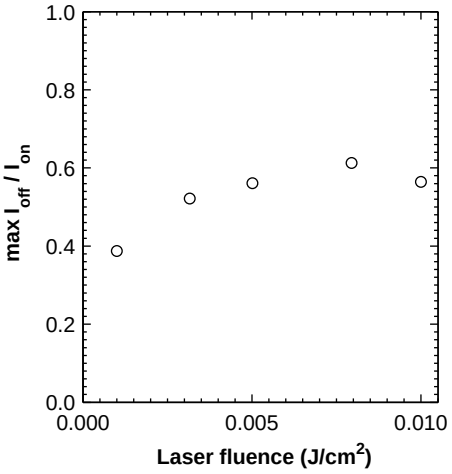

Fig. 9 Maximum off-wavelength to on-wavelength measurements ratio as a function of laser fluence.

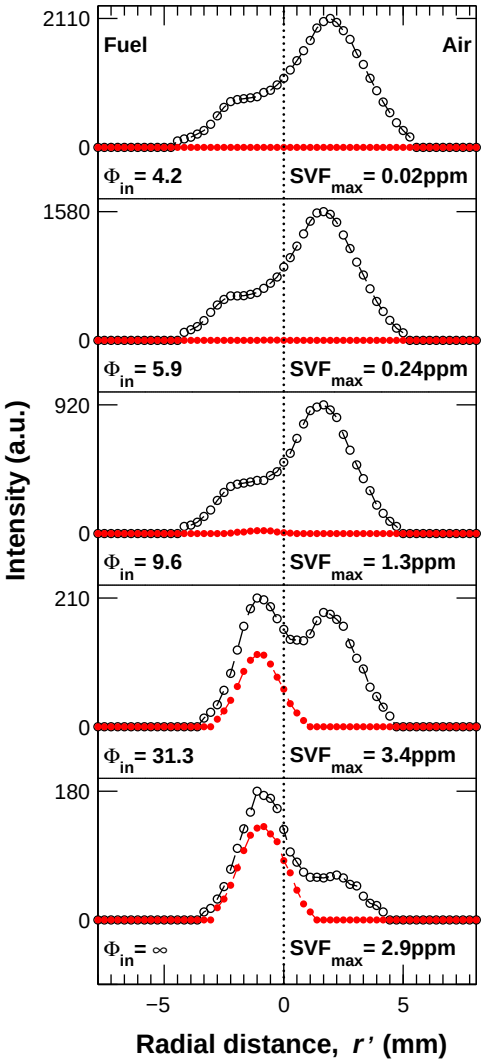

Fig. 10 Averaged radial profiles as a function of radial distance from peak soot volume fraction location, extracted at a HAB of 25 mm in Flame 1 to 5 (Table 1). Anti-Stokes process. Open circles: on-wavelength measurements. Dots: off-wavelength measurements. Vertical dotted line: peak soot volume fraction location.

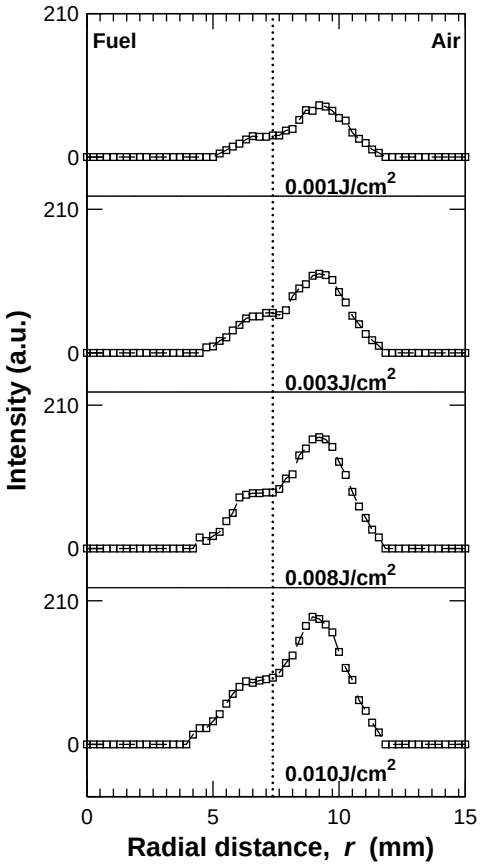

Fig. 11 Averaged radial profiles for the corrected on-wavelength measurements at four different laser fluences, extracted at a HAB of 25 mm in Flame 2 (Table 1). Anti-Stokes process.

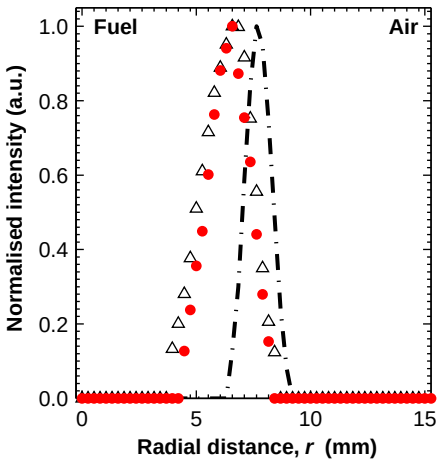

Fig. 12 Averaged radial profiles for extracted at a HAB of 25mm in Flame 1 (Table 1). Anti-Stokes process. Dashed line: soot volume fraction. Dots: off-wavelength measurements. Triangles: off-resonance measurements. These radial profiles have been normalised arbitrarily to their peak values.

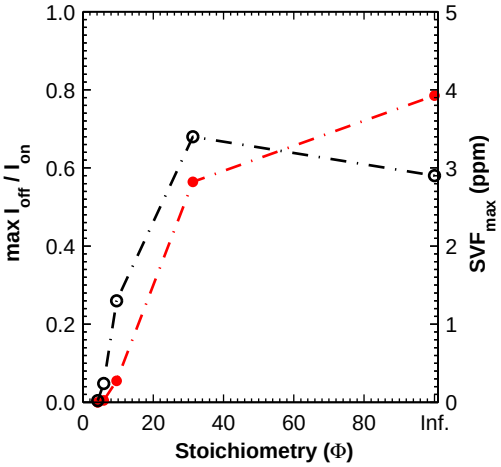

Fig. 13 Comparison of the maximum off-wavelength to on-wavelength measurements ratio (anti-Stokes) and maximum soot volume fraction at different flame stoichiometries (Φ). Dots: maximum off-wavelength to on-wavelength measurements ratio. Open circles: maximum soot volume fraction.